Bioactive Materials 40 (2024) 474–483

Contents lists available at ScienceDirect

Bioactive Materials

journal homepage: www.keaipublishing.com/en/journals/bioactive-materials

In situ engineered magnesium alloy implant for preventing postsurgical tumor recurrence

Wanying Li [a,b], Yinghui Wang [a,b,*], Chaojie Che [a], Xinyu Fu [a,b], Yang Liu [a,b], Dongzhi Xue [a,b], Shuai Zhang [d], Rui Niu [a,b], Hao Zhang [a,b], Yue Cao [d], Shuyan Song [a,b], Liren Cheng [a,**], Hongjie Zhang [a,b,c,***]

[a] State Key Laboratory of Rare Earth Resource Utilization, Changchun Institute of Applied Chemistry, Chinese Academy of Sciences, Changchun, Jilin, 130022, PR China
[b] School of Applied Chemistry and Engineering, University of Science and Technology of China, Hefei, Anhui 230026, PR China
[c] Department of Chemistry, Tsinghua University, Beijing, 100084, PR China
[d] The First Hospital of Jilin University, Changchun, Jilin, 130022, PR China

ARTICLE INFO

Keywords:
Magnesium alloy
Gas therapy
Mild magnetic hyperthermia therapy
Postsurgical tumor recurrence

ABSTRACT

Invasive tumors are difficult to be completely resected in clinical surgery due to the lack of clear resection margins, which greatly increases the risk of postoperative recurrence. However, chemotherapy and radiotherapy as the traditional means of postoperative adjuvant therapy, are limited in postoperative applications, such as multi-drug resistance and low sensitivity, etc. Therefore, an engineered magnesium alloy rod is designed as a postoperative implant to completely remove postoperative residual tumor tissue and inhibit tumor recurrence by gas and mild magnetic hyperthermia therapy (MMHT). As a reactive metal, magnesium alloy responds to the acidic tumor microenvironment by continuously generating hydrogen. The in-situ generation of hydrogen not only protects the surrounding normal tissue, but also enables the magnesium alloy to achieve MMHT under low-intensity alternating magnetic field (AMF). Furthermore, the numerous reactive oxygen species (ROS) produced by heat stress will combine with nitric oxide (NO) generated in situ, to produce more toxic reactive nitrogen species (RNS) storm. In summary, engineered magnesium alloy can completely remove residual tumor tissue and inhibit tumor recurrence by MMHT and RNS storm under low-intensity AMF, and the biodegradability of magnesium alloy makes great potential for clinical application.

1. Introduction

Surgical resection is the main means of clinical treatment for cancer. However, the effect of surgery is not satisfactory for many advanced cancers owing to its indistinguishable surgical margin, such as gastric cancer, lung cancer, breast cancer, etc. The residual microtumors after surgery, known as microscopic residual diseases (MRD), will lead to the huge risk of recurrence [1,2]. Therefore, postoperative radiotherapy and chemotherapy are the main methods to eliminate MRD in clinic. However, the treatment effect is still unsatisfactory due to the high systemic toxicity and low sensitivity. Recently, the postoperative treatments in situ have attracted extensive attention, for example, loading the chemotherapeutic drugs [3,4] or photosensitive molecules [5] in hydrogels for achieving chemotherapy or photodynamic therapy. However, there are still some challenges in completely eliminating MRD due to multi-drug resistance, the short lifetime of reactive oxygen species (ROS), and the poor penetration depth of light. As a result, it is urgent to explore a safe and effective orthotopic method after surgery for eliminating MRD and inhibiting the recurrence of tumor.

Magnetic hyperthermia therapy (MHT), a therapeutic method to eliminate tumor with the heat generated by magnetic nanoparticles under an alternating magnetic field (AMF), has gradually attracted attention due to the advantages of non-invasive, safe and unlimited penetration depth [6]. However, magnetic nanoparticles inevitably

Peer review under responsibility of KeAi Communications Co., Ltd.
* Corresponding author.
** Corresponding author.
*** Corresponding author. State Key Laboratory of Rare Earth Resource Utilization, Changchun Institute of Applied Chemistry, Chinese Academy of Sciences, Changchun, Jilin, 130022, PR China.
E-mail addresses: yhwang@ciac.ac.cn (Y. Wang), lrcheng@ciac.ac.cn (L. Cheng), hongjie@ciac.ac.cn (H. Zhang).

https://doi.org/10.1016/j.bioactmat.2024.06.004
Received 12 January 2024; Received in revised form 26 April 2024; Accepted 1 June 2024

accumulate in normal tissues through the systemic blood circulation, resulting in the thermal injury of normal tissues. What's more, high temperature promotes tumor cells to express heat shock proteins, which play a role in repairing damaged proteins and protecting existing proteins, making tumor cells insensitive to high temperature [7–11]. Therefore, more safe and effective magnetic heating agents need to be explored. Magnesium alloy is a biodegradable implant approved by European standards and Korea Food and Drug Administration [12,13], which degrades in the acidic tumor microenvironment (TME) to produce safe magnesium ions and hydrogen. And surprisingly, due to the low resistivity of the bulk metal, magnesium alloy will produce a large eddy current under AMF to further generate heat, and therefore has recently been reported as a magnetic heating agent [14,15]. More importantly, as an active metal, magnesium can produce hydrogen gas in TME [16]. Large amounts of hydrogen will inhibit the mitochondrial respiration of cancer cells and further inhibit ATP production, leading to down-regulation of the expression of heat shock proteins and sensitize cancer cells to relative low temperature [17,18]. Therefore, magnesium alloy could be act as a promising agent for mild magnetic hyperthermia therapy (MMHT).

Nitric oxide (NO), an important biological mediator, could kill cancer cells through causing the mitochondrial and DNA injury at high concentration [19]. Moreover, NO can react with ROS to produce more toxic reactive nitrogen species (RNS), improving the treatment effect. Excitingly, MMHT can not only inhibit proliferation of cancer cells, but also induce high level of ROS in tumor site [20,21]. Therefore, gas therapy could significantly enhance the efficacy of MMHT in removing MRD and preventing tumor recurrence. However, to the best of our knowledge, there is no report on the magnesium alloy material that combines MMHT and gas therapy for highly efficient MRD elimination. What's more, it is still a challenge to achieve the "precise" delivery and release of NO in the tumor site. Among various NO donors [22–24], poly-L-arginine (PL-Arg) has attracted attention due to its good biosafety and excellent NO production. L-arginine, as a monomer of PL-Arg, is an endogenous essential amino acid and can be oxidized to produce NO [25]. But due to the limited hydrogen peroxide (H_2O_2) content in the TME, the production of NO is not satisfactory. Therefore, it is highly desired to developed magnesium alloy composites with oxidation properties for further improving NO production.

Here, we first constructed a magnesium alloy composites based on Mg–Zn–Ca alloy (MgA) rod with good biological safety, approved by the KFDA for clinical application in 2015. As shown in Scheme 1, magnesium peroxide (MgO_2) shell was in situ grown on the surface of MgA rod (MgA@MgO_2, MM), followed by loading with bovine serum albumin (BSA) and PL-Arg (MgA@MgO_2@BSA@PL-Arg, MMBP). MMBP exhibited the good performance of MMHT under low-intensity AMF. In the acidic TME, the MgO_2 shell will degrade first to produce excessive H_2O_2, triggering PL-Arg to generate NO. In the meantime, NO further reacts with ROS induced by MMHT to produce highly toxic RNS. Importantly, hydrogen produced in the TME can further protect the surrounding normal tissues from heat-induced inflammation [26]. When the AMF was removed, MMBP would inhibit tumor recurrence continuously. To the best of our knowledge, this is the first report on the magnesium alloys nanocomposite for effectively eliminating MRD and inhibiting tumor recurrence.

2. Results and discussion

2.1. Preparation and characterization of MMBP

The growth of MgO_2 on the MgA rod was based on the preparation method of MgO_2 in industry. MgA was first immersed in saturated sodium bicarbonate solution, then calcined at 500 °C, and finally immersed in H_2O_2 solution. Scanning electron microscopy (SEM) images

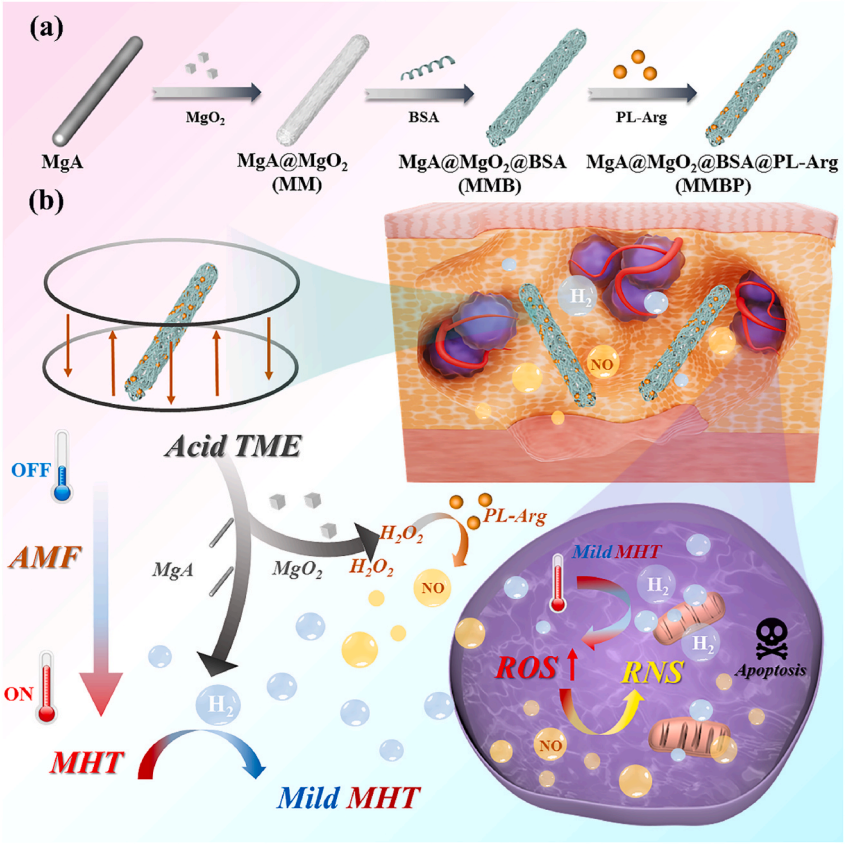

Scheme 1. **(a)** The synthesis process of MMBP. **(b)** MMBP for gas/mild magnetic hyperthermia therapy.

and digital photographs showed that the surface of MgA was significantly rougher, and the metallic luster decreased (Fig. 1a and Fig. S1). To further verify the structure of the surface coating, the powder grown on the MgA was scraped off for X-ray diffraction (XRD) analysis. The characteristic peaks at 37.1° and 53.8° in the XRD pattern correspond to (200) and (220) of the cubic structure of MgO_2, respectively, indicating that MgO_2 was successfully synthesized (JCPDS. 19–0771, Fig. 1b) [27]. In addition, the characteristic infrared absorption peaks of 669 cm^{-1} and 866 cm^{-1} in the Fourier-transform infrared (FTIR) spectra correspond to Mg–O and O–O binds of MgO_2, respectively (Fig. 1c) [28]. According to Figure S2 and Fig. 2d, the main peaks in the O1s X-ray photoelectron spectroscopy (XPS) spectrum was significantly shifted, demonstrating the change of the valence of the oxygen [29]. To further verify the synthesis mechanism of MgO_2, we characterized the intermediate products. In Fig. S3a, the characteristic peaks in XRD patterns demonstrated that magnesium carbonate trihydrate was formed on the MgA soaked in saturated sodium carbonate. Similarly, after calcination of magnesium carbonate trihydrate at 500 °C, MgO was generated as shown in the XRD patterns of Fig. 1b. What's more, the XRD patterns of MgA@MgO and MgA@MgO_2 (MM) were supplemented in Fig. S3b. The above results illustrate the successful coating MgO_2 on the surface of MgA. Then, BSA was adsorbed to the surface of the MM through the chelation of the carboxyl group in BSA with Mg^{2+}. The SEM images (Fig. 1a) showed that the surface of the BSA-modified MM became rougher than MM, and the digital photograph showed that the MM turned white, demonstrating that BSA was attached to the MM and successfully synthesized MgA@MgO_2@BSA (MMB). Furthermore, the NO donor was adsorbed on the MMB by the electrostatic adsorption of BSA and the PL-Arg. As shown in Fig. 1e, the zeta potential of powder scraped from the surface of MMB is about −19.1 mV, and that of free PL-Arg is about 10.74 mV, while the potential of powder scraped from the surface of MMBP increases from −19.1 mV to −9.38 mV. The change of zeta potential indicates that the successful loading of PL-Arg. Finally, the loading rates of MgO_2, BSA and PL-Arg on the MgA substrate were calculated to be about 2.66 %, 3.32 % and 1.45 % by thermogravimetric analysis (TGA), respectively (Fig. 1f).

2.2. MMBP generates H_2 and NO and achieves MMHT

MgA can produce hydrogen in the acidic TME [16]. To verify the property of hydrogen production by MMBP, methylene blue (MB) was used to detect the short-term release of hydrogen, and gas chromatography was used to quantify the long-term release. MB was used as a probe because MB would be reduced by hydrogen to colorless leucomethylene blue (leucoMB) under the catalysis of Pt and the peak absorption of MB at 663 nm will be reduced [30]. As shown in Fig. 2a, MMBP of the same length was immersed in PBS at pH 6.5 and PBS at pH 7.4 as the experimental group and the control group, respectively. MB in the experimental group became colorless while that in the control group remained blue, verifying the good ability of MMBP to produce hydrogen

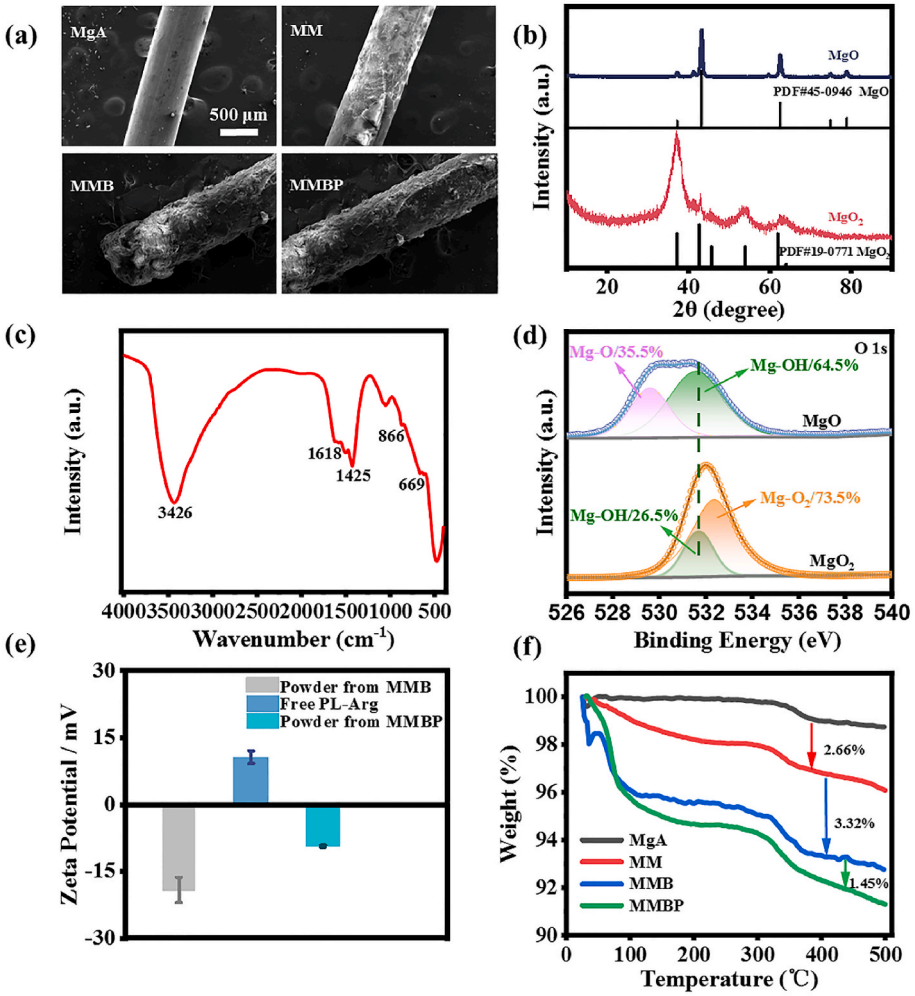

Fig. 1. Characterizations of MMBP. **(a)** The SEM images of MgA, MM, MMB and MMBP. **(b)** The XRD patterns of magnesium oxide (MgO) and MgO_2. **(c)** The FTIR spectra of MgO_2. **(d)** The XPS spectrum of MgO and MgO_2. **(e)** The zeta potential of the powder from MMB, free PL-Arg and the powder on the surface of MMBP. **(f)** The TGA results of MgA, MM, MMB and MMBP.

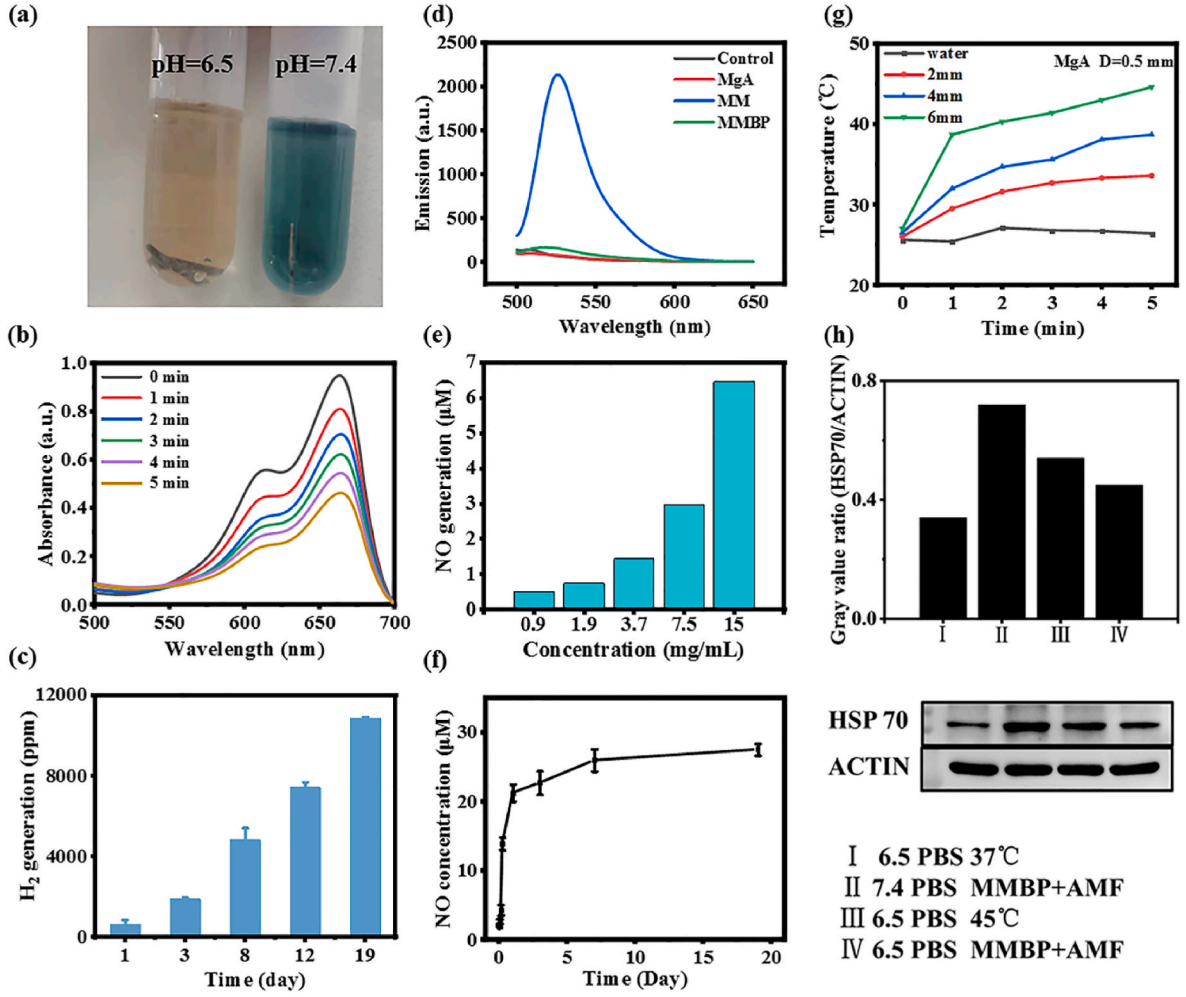

Fig. 2. **(a)** Digital photographs of experimental (pH = 6.5) and control groups (pH = 7.4). **(b)** Measurement of hydrogen generation by magnesium alloys for a short time. **(c)** Measurement of hydrogen generation by magnesium alloys over a long time. **(d)** The generation and consumption of H_2O_2. **(e)** The NO generation by MMBP with different PL-Arg concentrations. **(f)** The NO generation by MMBP with time. **(g)** The temperature of MgA (D = 0.5 mm) with time under the AMF ($H_{appl} \times f_{appl} = 1.84 \times 10^8$ A m$\cdot^{-1}\cdot$s^{-1}). **(h)** The expression of HSP70 in tumor cells with different treatments (In groupIIand IV, $H_{appl} \times f_{appl} = 1.84 \times 10^8$ A m$\cdot^{-1}\cdot$s^{-1}, 5 min).

in acidic environment. The UV–vis absorption spectrum (Fig. 2b) also showed that the absorption value of MB at the characteristic peak of 663 nm (MB) continuously decreased with time, which further proved the ability of MMBP to release hydrogen in the acidic environment. Furthermore, the total amount of hydrogen produced by MMBP over different days was collected and quantified by gas chromatography. It was found that the hydrogen production capacity of MMBP did not decrease within 19 days, indicating the potential of MMBP in long-term inhibition of tumor recurrence (Fig. 2c). Then, the ability of MM to produce H_2O_2 was verified with 2′,7′-Dichlorodihydrofluorescein (DCFH) as a probe. DCFH will be oxidized by H_2O_2 to become 2′, 7′-dichlorofluorescein (DCF), which showed a distinct emission peak at 529 nm, while the emission peak at 529 nm was significantly attenuated in the MMBP group (Fig. 2d). It was proved that MgO_2 was degraded to produce H_2O_2, which was then consumed. Thereafter, the Griess reagent was used to verify the NO production capability of MMBP. As shown in Fig. 2e, the production of NO increased with the increase of PL-Arg concentration, proving that PL-Arg loading on the surface of MMBP can be oxidized by H_2O_2 from decomposition of MM core in acidic PBS. Subsequently, MMBP was mixed with acidic PBS to detect NO production at different time points. It was found that within 24 h, the production of NO increased with time, indicating that MMBP could continuously release NO for a long time in acidic environment and reach a high concentration of 21.82 μM (Fig. 2f). What's more, in order to quantitatively study the magneto-thermal conversion property of MgA, we recorded the temperature of MgA rods with different lengths and diameters in 96-wells plate under the AMF ($H_{appl} \times f_{appl} = 1.84 \times 10^8$ A m$\cdot^{-1}\cdot$s^{-1}). The intensity and frequency of the AMF are much lower than the limit of the applied magnetic field for magnetic heating therapy ($H_{appl} \times f_{appl} = 5 \times 10^9$ A m$\cdot^{-1}\cdot$s^{-1}) [31]. In Fig. 2g and Figs. S4a and b, with the increase of AMF application time, length and diameter of MgA rods, the temperature of PBS in the well continues to rise, which can be heated up to 86.1 °C within 5 min. At the same time, the magneto-thermal conversion ability of MgA did not change after four cycles of heating and cooling (Fig. S4c). Then, the temperatures of MgA group, MM group and MMBP group were basically same under the same condition (Fig. S4d), indicating that the surface modification of MgA has no effect on its heating performance. All the results illustrated the potential of MgA in magneto-thermal therapy. However, high temperature will definitely damage the surrounding normal tissues, so MMBP with a diameter of 0.5 mm and a length of 6 mm was selected for treatment (Fig. 2g). As shown in Fig. 2h, both group II and group IV of tumor cells were treated with AMF for 5 min. However, the HSP70 expression in group II cells was higher than that in group III cancer cells treated with PBS at 45 °C, while the opposite was observed in group IV. This results showed that hydrogen produced by MgA in acidic condition indeed downregulated the expression of HSP70 in tumor cells, which is beneficial to realize MMHT.

2.3. MMBP effectively kills tumor cells through gas therapy and MMHT

Encouraged by the excellent abilities of H_2 production, NO production and magneto-thermal conversion of MMBP, we further validated its MRD clearance ability in vitro. Various aggressive cancer cells including mouse breast cancer cells (4T1), mouse gastric cancer cells (MFC) and Human A549 cells (A549) were selected to verify the effect of MRD clearance of MMBP. As shown in Fig. 3a, the survival rate of cancer cells incubated with MgA was significantly decreased compared with the control group, proving that the generated H_2 effectively inhibit the

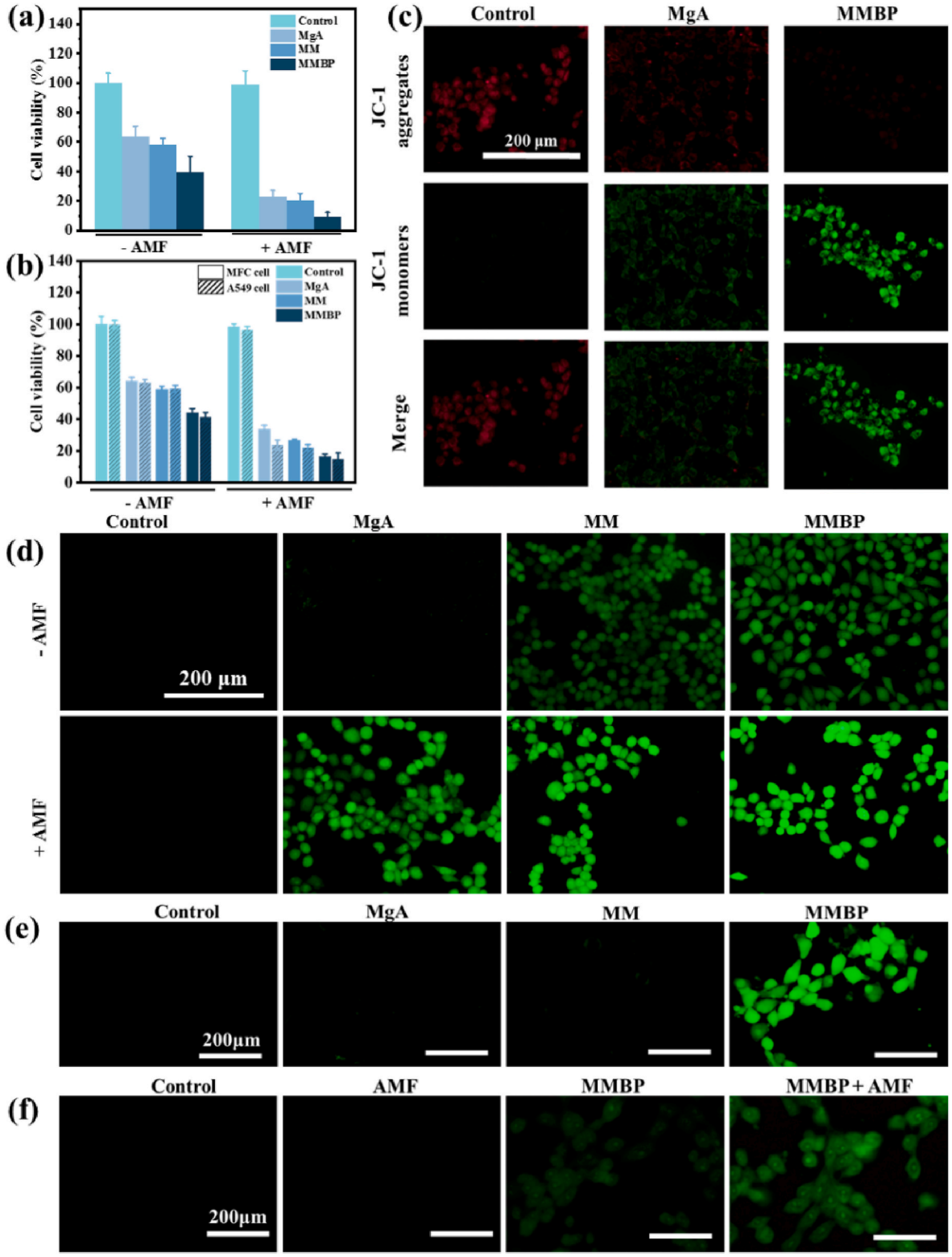

Fig. 3. Treatment effect of MMBP. (a) The therapeutic effect of MgA, MM and MMBP on 4T1 cells. **(b)** The therapeutic effect of MgA, MM and MMBP on MFC cells and A549 cells. **(c)** Changes of mitochondrial membrane potential in 4T1 cells treated with MgA and MMBP. **(d)** The detection of ROS in 4T1 cells. **(e)** The detection of NO in 4T1 cells. **(f)** The detection of RNS in 4T1 cells.

proliferation of tumor cells. Compared with MM-treated group cells, the cell viability of MMBP-treated group cells decreased more significantly, indicating that the better treatment effect of H_2 combined with NO than that of H_2 alone. The significant reduction of cell viability in each group treated with AMF demonstrate the excellent efficacy of combined gas/mild magnetic hyperthermia therapy. Similarly, the proliferation of MFC and A549 cells was also inhibited in the same condition (Fig. 3b), suggesting the therapeutic ability of the material is not limited to a single type of cell, and has a wide range of therapeutic prospects. We also demonstrated the biocompatibility of MMBP by mouse fibroblasts cells (L929) cells. As shown in Fig. S5, the viability of the cells in all groups was greater than 85 %, proving the excellent biocompatibility of the material for normal cells. It is known that H_2 and NO can inhibit respiration of cancer cells and further disrupt mitochondrial structure. 5, 5′, 6, 6′- Tetrachloro - 1, 1′, 3, 3′- tetraethylimidacarbocyanine (JC-1) was employed to detect mitochondrial membrane potential changes. As

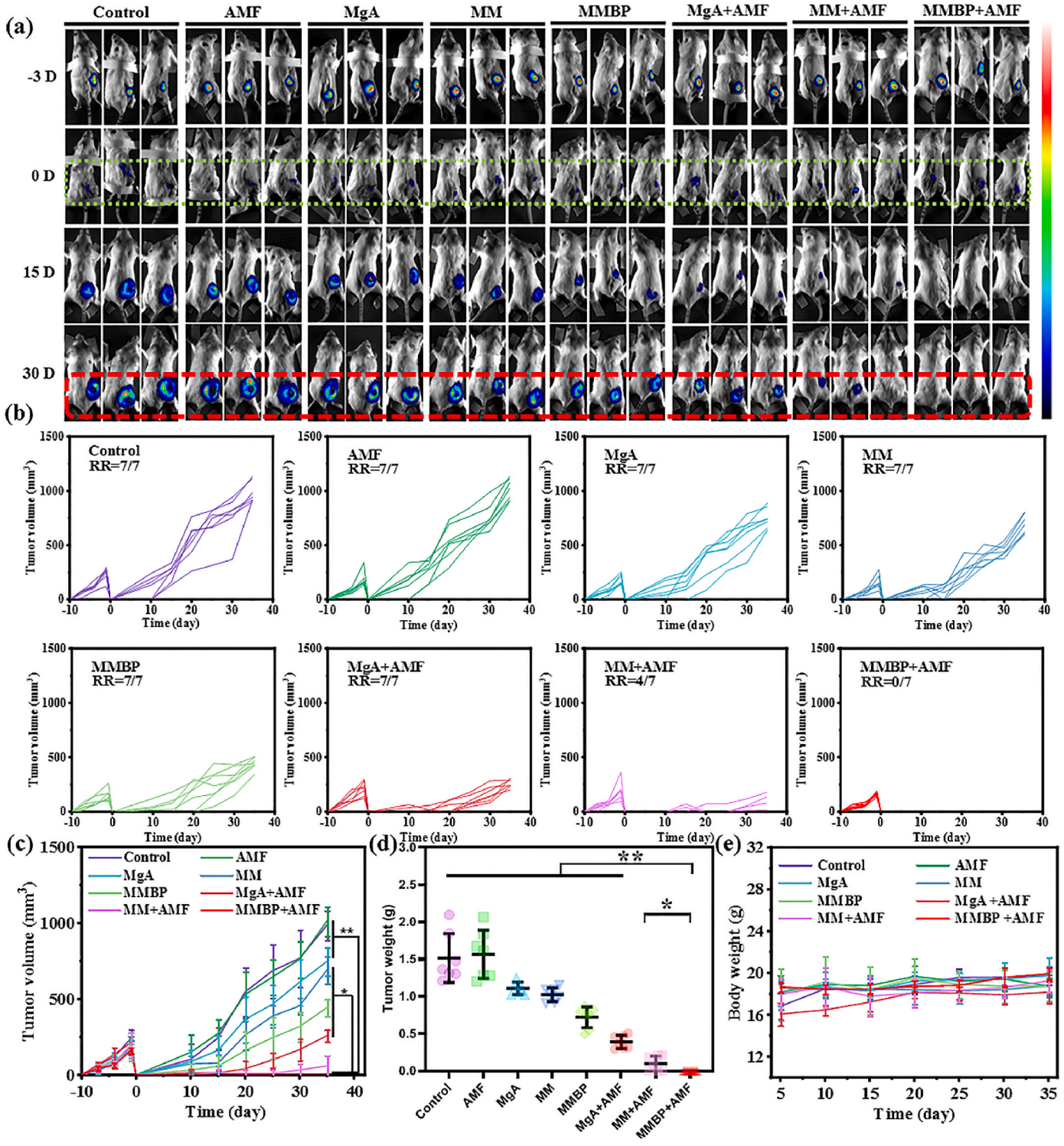

Fig. 4. **(a)** The bioluminescence images of mice treated with MgA, MM and MMBP. **(b)** Tumor recurrence in all groups of mice. **(c)** The volume of recurrent tumors in each group of mice. **(d)** The quality of recurrent tumors in each group of mice. **(e)** Curve of body weight change in each group of mice.

expected, the cells treated with MgA showed weak green fluorescence, whereas the cells treated with MMBP showed markedly enhanced green fluorescence (Fig. 3c), indicating that H_2 and NO damaged the mitochondria, leading to a decrease in mitochondrial membrane potential. Subsequently, the intracellular ROS was evaluated via the dichlorodihydrofluorescein diacetate (DCFH - DA) staining experiment. As shown in Fig. 3d and S6a, cells treated with MgA showed no obvious fluorescence, however, cells in the MM group showed weak green fluorescence, which could be attributed to the generation of H_2O_2 from MM. The apparent increase of fluorescence intensity in MMBP-treated cells, ascribing to the generation of NO and RNS [32]. Meanwhile, NO could consume excessive glutathione in cancer cells, leading to an increase in intracellular ROS level [33]. In addition, the increase of fluorescence intensity in each group after AMF application proved that the excessive heat stress-initiated ROS was produced in cancer cells under overheating conditions. Moreover, the production of NO and nitrite peroxide (ONOO•) were verified by fluorescence staining experiments. The 3-Amino,4-aminomethyl-2′,7′-difluorescein diacetate (DAF-FM DA) staining result showed that there was no green fluorescence in MgA group and MM group. Only the MMBP-treated group exhibited strong green fluorescence (Fig. 3e and S6b), which proved that the NO was produced in the MMBP group. The result of DAX-J2 PON Green staining revealed that the cells treated with MMBP- emitted weak green fluorescence, and the stronger green fluorescence was observed in MMBP + AMF group, indicating that the magnetic heating treatment increased the intracellular ROS level and promoted the production of ONOO• (Fig. 3f and S6c). Finally, calcein AM/propidium iodide staining experiment and apoptosis experiment were used to further verify the combined therapeutic effect of MMHT and gas therapy (Figs. S7a and b). It was found that almost all cells in MMBP + AMF group were stained red, and the proportion of apoptosis was about eight times that of control group, indicating that RNS storm generated by MMHT and gas combined therapy had excellent tumor cell killing effect.

2.4. MMBP effectively **eliminate MRD and** inhibits tumor recurrence after surgery

To mimic the MRD in clinic, we excised tumor tissue from Luc-4T1-bearing mice and left approximately 10 % residual tumor tissue to verify the ability of MMBP to clear MRD and inhibit tumor recurrence in vivo. MgA, MM, and MMBP were implanted to the residual tumor tissue of mice after surgery and AMF would be applied for treatment on day 5 and day 10 post the operation, respectively. Then, the bioluminescence was employed to record the residual tumor tissues, which exhibits the tumor recurrence clearly and intuitively. As shown in Fig. 4a, in the Control and AMF groups, tumor recurrence was observed on the 15th day after surgery. The volume of recurrent tumors in the MgA and MM groups was smaller than that in both Control and AMF groups on postoperative day 15, indicating that hydrogen can inhibit tumor growth to a certain extent, but could not completely inhibit tumor recurrence. Similarly, there was little tumor recurrence in MgA + AMF group and MM + AMF group on the 15th day after surgery, but tumor recurrence was obvious on postoperative day 30, indicating that the effect of inhibition tumor recurrence of MMHT is not satisfactory. However, mice in the MMBP + AMF group did not show tumor recurrence at either postoperative day 15 or day 30, indicating that gas therapy significantly enhanced the therapeutic effect of mild magnetic heating therapy, which can effectively eliminate MRD. At the same time, the volume and mass of recurrent tumors in each group were monitored during the treatment (Fig. 4b, c and d) and the results were consistent with the bioluminescence imaging. And the slightly increased body weight of the mice indicates the MgA nanocomposites had no obvious acute adverse effect on the mice during the treatment (Fig. 4e).

In order to further verify the mechanism of the elimination of MRD in vivo by the combination of MMHT and gas therapy, the tumor temperature of mice at different time points was determined by a near infrared camera. As shown in Fig. 5a and b, the temperature of tumor tissue implanted with MgA under AMF exceeded 40 °C at 4min and 45 °C at 5min, indicating MMHT was achieved successfully. Then, the content of NO in the tumor was measured. As shown in Fig. 5c, the concentration of NO in the tumor tissue treated with MMBP was significantly increased. Furthermore, according to the staining results of tumor tissue sections (Fig. 5d and e), ROS and RNS in tumor tissue of mice treated by MMBP + AMF were significantly increased, demonstrating the successful combination of MMHT and NO treatment. Meanwhile, TUNEL and Ki-67 staining of different treated tumour tissues showed that MMHT and gas therapy successfully inhibited the proliferation of tumour cells and greatly promoted their apoptosis (Fig. 5f and Fig. S8).

Finally, to verify that hydrogen prevented tumor recurrence, we surgically removed intact tumor tissue from six mice inoculated with Luc-4T1 cell, instead of 10 % remaining tumor tissue. Mice after surgery were randomly divided into two groups, one of which was implanted with MgA instead of MMBP to verify the effect of hydrogen on preventing recurrence. The tumor recurrence at the surgical site was observed by bioluminescence, and the weight changes of the two groups of mice were recorded within 40 days. As shown in Fig. 5g, there was no significant tumor recurrence in both groups of mice within 20 days after surgery. However, on day 30 after surgery, recurrent tumor tissue was observed in control mice without hydrogen intervention. The mice implanted with MgA did not show tumor recurrence until the 40th day after surgery and the weight of the mice showed a steady upward trend (Fig. S9), indicating that the material implantation had no significant effect. The above shows that hydrogen gas can inhibit tumor recurrence in the long term.

2.5. Degradability and biosafety of MMBP

Furthermore, we tested the biodegradability of MgA by mixing it with normal saline solution, deionized water and PBS at pH 7.4 and pH 6.5, respectively, and implanted MgA subcutaneously into healthy mice for 90 days. The changes in surface appearance and quality of MgA were recorded (Fig. 6a and b). MgA showed a mass loss of approximately 70 % after 90 days in PBS at pH 6.5 and more than 20 % after 90 days in normal tissues in vivo. The above results indicate that MgA is degraded rapidly in acidic TME and continues to be degraded slowly in normal tissues. Therefore, when the MRD is completely removed, the MgA will continue to degrade slowly in the normal physiological environment, demonstrating that the MgA do not need to be removed again and protect the patients from secondary damage. Finally, we further verified the biological safety of MgA. We analyzed the Mg^{2+} content in the main organs of mice implanted with MgA for different days, and found that there was no abnormal Mg^{2+} content (Fig. 6c). At the same time, as shown in Fig. 6d, hematoxylin-eosin (H&E) staining results of major organs were normal, with no obvious damage. In addition, the blood analysis results of mice treated with MMBP (Fig. S10) were basically consistent with those of the control group, both within the normal range, indicating that MMBP had good biosafety.All the above demonstrate that MMBP can not only be degraded to reduce the harm to patients, but also show great biosafety, exhibiting great potential in clinical application to clear MRD and inhibit cancer recurrence.

3. Conclusion

In summary, we synthesized a biodegradable MMBP to successfully remove MRD and long-term inhibit tumor recurrence after surgery by mild magnetic hyperthermia/combination gas therapy. In the acidic TME, MMBP can achieve MMHT with the assistance of hydrogen generated in situ, which can reduce the thermal damage to the surrounding normal tissues. Then, NO produced in situ by MMBP significantly enhanced the therapeutic efficacy of MMHT on MRD clearance and long-term tumor recurrence, as NO would combine with ROS produced by heat stress to generate more toxic RNS. Finally, MMBP shows

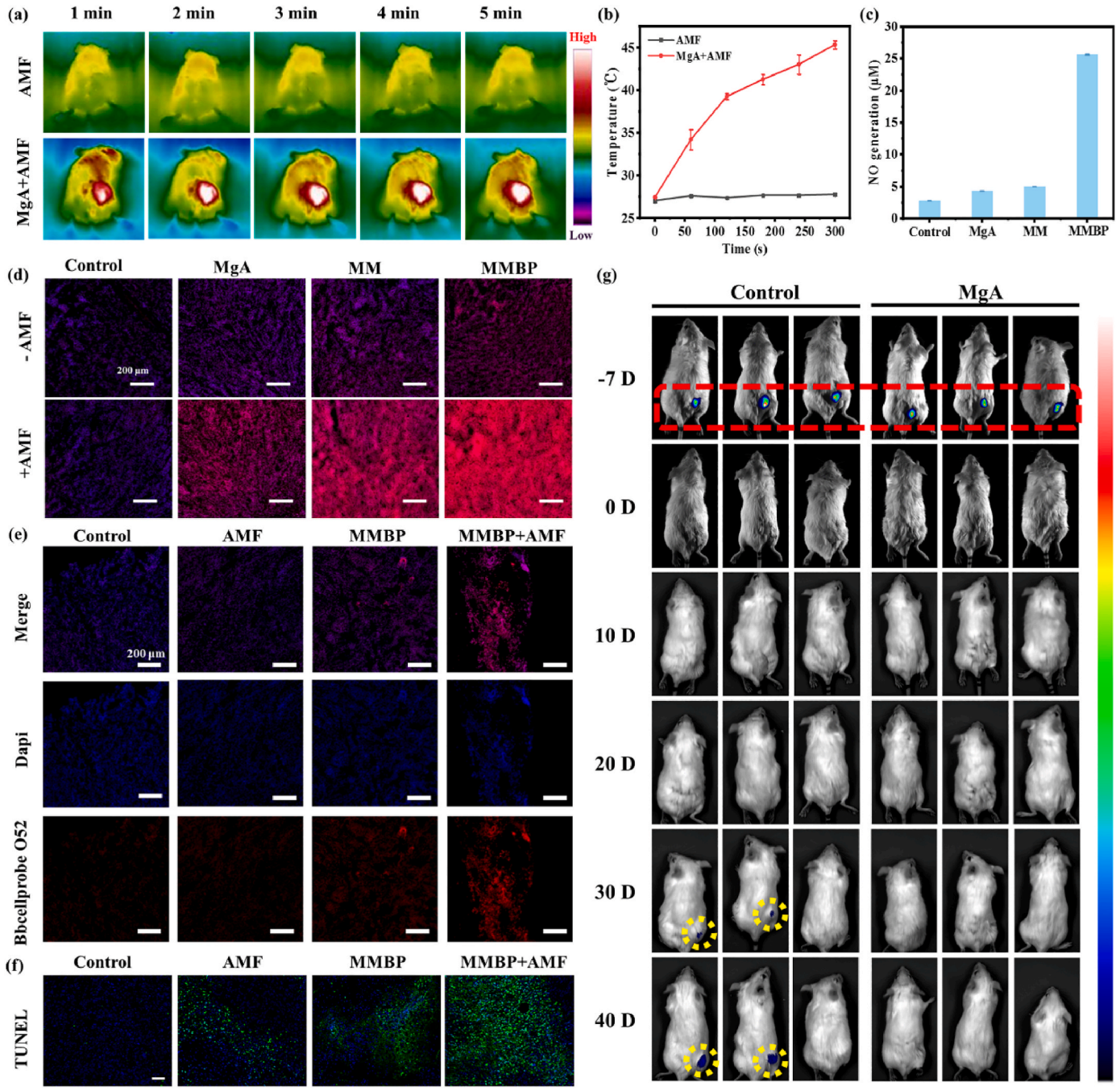

Fig. 5. (a–b) Determination of intratumoral temperature in mice under alternating magnetic field. (c) The concentration of NO in tumor of mice treated with MgA, MM and MMBP. (d) ROS staining in tumor of mice. (e) RNS staining in tumor of mice. (f) TUNEL staining in tumor of mice. (g). The bioluminescence images of postoperative mice treated with MgA.

excellent biosafety and rapid degradation in tumors, but slow degradation in normal tissues, which makes MMBP show great potential as an adjuvant therapeutic material for postoperative recovery. This work provides a new perspective for the elimination of postoperative MRD and the long-term suppression of postoperative tumor recurrence.

4. Experimental methods

4.1. Synthesis of MM

Firstly, the MgA was immersed in saturated sodium bicarbonate solution overnight, then it was removed and cleaned with deionized water. Then, the MgA was calcined in a muffle furnace at 500 °C for 3 h. Lastly, the rod was immersed in hydrogen peroxide solution overnight and MM was obtained.

4.2. Synthesis of MMBP

BSA was dispersed in PBS at pH 7.4 to ensure that the solution keep neutral, and MM rods were immersed in the above solution overnight at room temperature. The MMB was obtained. Similarly, ploy-L-argine hydrochloride was dissolved in PBS at pH 7.4 to ensure that the solution keep neutral, and the MMB rod was then immersed in the solution overnight at room temperature. The MMBP was obtained successfully.

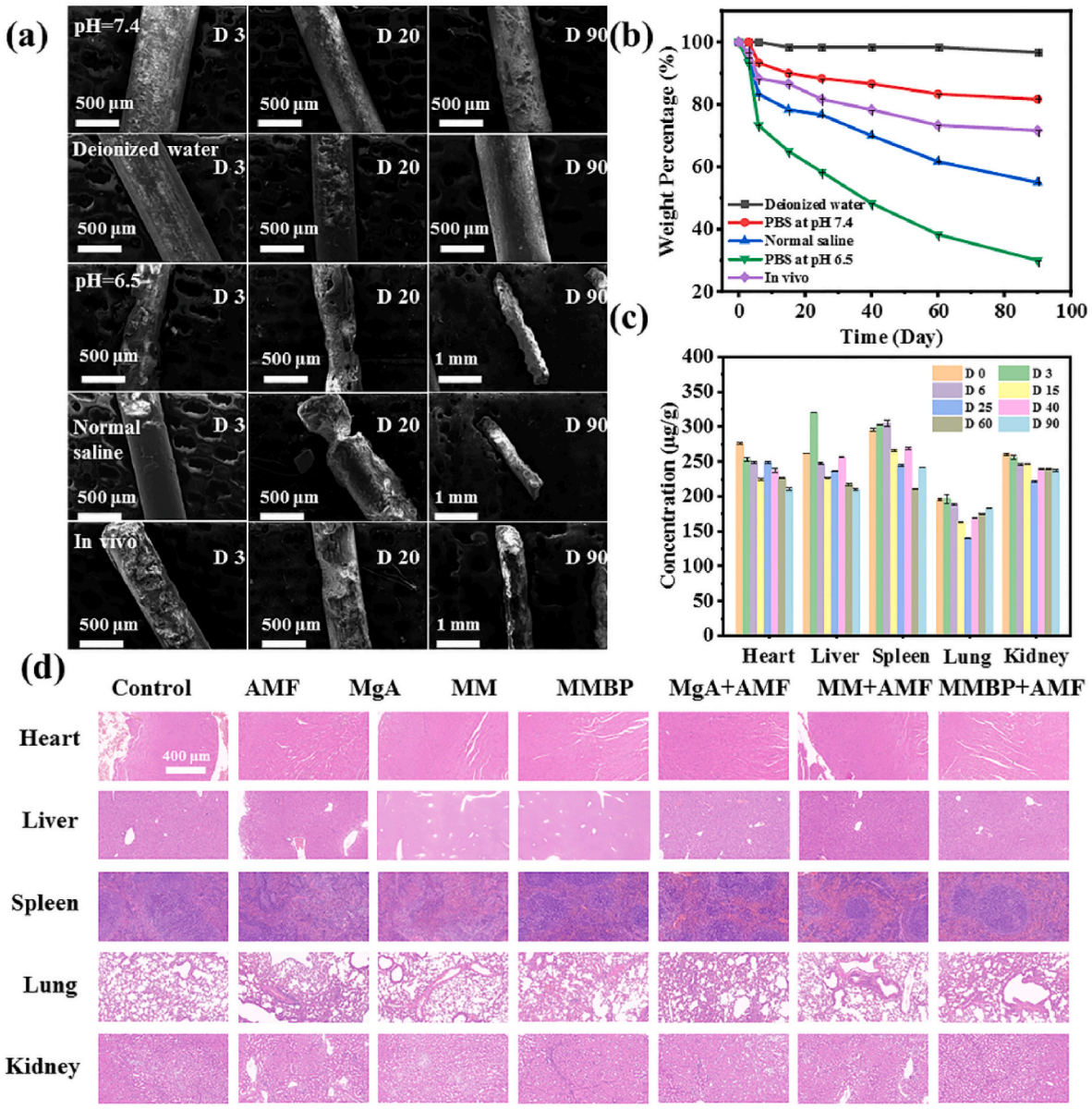

Fig. 6. **(a)** Surface morphologies of MgA rods during 90 days. **(b)** Mass change of MgA rods treated with different conditions. **(c)** Changes of Mg^{2+} content in major organs of mice. **(d)** H&E staining images of major organs.

4.3. The characterization

Detailed procedures for material characterization, cell experiments, and in vivo experiments can be found in Supporting information.

Ethics approval and consent to participate

All of the animal experiments were conducted according to the rules of the Ethics committee of Changchun Chemical Institute (20220001).

CRediT authorship contribution statement

Wanying Li: Writing – original draft, Validation, Supervision, Methodology, Investigation, Conceptualization. **Yinghui Wang:** Writing – review & editing, Supervision, Conceptualization. **Chaojie Che:** Methodology, Investigation. **Xinyu Fu:** Validation. **Yang Liu:** Visualization. **Dongzhi Xue:** Methodology. **Shuai Zhang:** Methodology. **Rui Niu:** Methodology. **Hao Zhang:** Software. **Yue Cao:** Methodology. **Shuyan Song:** Writing – review & editing, Conceptualization. **Liren Cheng:** Writing – review & editing, Supervision, Conceptualization. **Hongjie Zhang:** Writing – review & editing, Supervision, Conceptualization.

Declaration of competing interest

The authors declare that they have no known competing financial interests or personal relationships that could have appeared to influence the work reported in this paper.

Acknowledgements

This work was supported by the financial aid from the Basic Science Center Project of the National Natural Science Foundation of China (22388101), National Natural Science Foundation of China (Grant Nos. 22020102003, U23A20581, 52272169, and 52022094), National Key R&D Program of China (2020YFA0712102), the Program of Science and Technology Development Plan of Jilin Province of China (No. 20230508071RC) and the Youth Innovation Promotion Association of

Chinese Academy of Sciences (Grant 2019232).

Appendix A. Supplementary data

Supplementary data to this article can be found online at https://doi.org/10.1016/j.bioactmat.2024.06.004.

References

[1] D.Y. Wang, J.W. Liu, J. Duan, H. Yi, J.J. Liu, H.W. Song, et al., Enrichment and sensing tumor cells by embedded immunomodulatory DNA hydrogel to inhibit postoperative tumor recurrence, Nat. Commun. 14 (1) (2023) 4511, https://doi.org/10.1038/s41467-023-40085-4.

[2] E.Y. Lukianova-Hleb, Y.S. Kim, I. Belatsarkouski, A.M. Gillenwater, B.E. O'Neill, D. O. Lapotko, Intraoperative diagnostics and elimination of residual microtumours with plasmonic nanobubbles, Nat. Nanotechnol. 11 (6) (2016) 525, https://doi.org/10.1038/nnano.2015.343.

[3] Q. Lu, H. Ye, K. Wang, J. Zhao, H. Wang, J. Song, et al., Bioengineered platelets combining chemotherapy and immunotherapy for postsurgical melanoma treatment: internal core-loaded doxorubicin and external surface-anchored anti-PD-L1 antibody backpacks, Nano Lett. 22 (7) (2022) 3141–3150, https://doi.org/10.1021/acs.nanolett.2c00907.

[4] W. Chen, K. Shi, J. Liu, P. Yang, R. Han, M. Pan, et al., Sustained co-delivery of 5-fluorouracil and cis-platinum via biodegradable thermo-sensitive hydrogel for intraoperative synergistic combination chemotherapy of gastric cancer, Bioact. Mater. 23 (2023) 1–15, https://doi.org/10.1016/j.bioactmat.2022.10.004.

[5] Y. Zhang, S. Tian, L. Huang, Y. Li, Y. Lu, H. Li, et al., Reactive oxygen species-responsive and Raman-traceable hydrogel combining photodynamic and immune therapy for postsurgical cancer treatment, Nat. Commun. 13 (1) (2022) 4553, https://doi.org/10.1038/s41467-022-32160-z.

[6] H. Yan, W. Shang, X. Sun, L. Zhao, J. Wang, Z. Xiong, et al., "All-in-One" nanoparticles for trimodality imaging-guided intracellular photo-magnetic hyperthermia therapy under intravenous administration, Adv. Funct. Mater. 28 (9) (2018) 1705710, https://doi.org/10.1002/adfm.201705710.

[7] S. Dong, Y. Dong, Z. Zhao, J. Liu, S. Liu, L. Feng, et al., "Electron transport chain interference" strategy of amplified mild-photothermal therapy and defect-engineered multi-enzymatic activities for synergistic tumor-personalized suppression, J. Am. Chem. Soc. 145 (2023) 9488–9507, https://doi.org/10.1021/jacs.2c09608.

[8] J. Cheng, L. Li, D. Jin, Y. Dai, Y. Zhu, J. Zou, et al., Boosting ferroptosis therapy with iridium single-atom nanocatalyst in ultralow metal content, Adv. Mater. 35 (2023) 2210037, https://doi.org/10.1002/adma.202210037.

[9] C. Zhang, D.-W. Zheng, C.-X. Li, M.-Z. Zou, W.-Y. Yu, M.-D. Liu, et al., Hydrogen gas improves photothermal therapy of tumor and restrains the relapse of distant dormant tumor, Biomaterials 223 (2019) 119472, https://doi.org/10.1016/j.biomaterials.2019.119472.

[10] M. Chang, Z. Hou, M. Wang, C. Yang, R. Wang, F. Li, et al., Single-atom Pd nanozyme for ferroptosis-boosted mild-temperature photothermal therapy, Angew. Chem., Int. Ed. 60 (23) (2021) 12971–12979, https://doi.org/10.1002/anie.202101924.

[11] H. Chen, B. Ding, J. Tan, P. Zheng, Z. Cheng, Pa Ma, et al., Palladium hydride nanourchins with amplified photothermal therapeutic effects through controlled hydrogen release and antigen-assisted immune activation, Chem. Eng. J. 442 (2022) 136296, https://doi.org/10.1016/j.cej.2022.136296.

[12] J.-W. Lee, H.-S. Han, K.-J. Han, J. Park, H. Jeon, M.-R. Ok, et al., Long-term clinical study and multiscale analysis of in vivo biodegradation mechanism of Mg alloy, Proc. Natl. Acad. Sci. U.S.A. 113 (3) (2016) 716–721, https://doi.org/10.1073/pnas.1518238113.

[13] H. Windhagen, K. Radtke, A. Weizbauer, J. Diekmann, Y. Noll, U. Kreimeyer, et al., Biodegradable magnesium-based screw clinically equivalent to titanium screw in hallux valgus surgery: short term results of the first prospective, randomized, controlled clinical pilot study, Biomed. Eng. Online 19 (1) (2020) 86, https://doi.org/10.1186/s12938-020-00818-8.

[14] X. Yang, N. Yang, L. Zhang, D. Zhao, H. Lei, S. Cheng, et al., Eddy current thermal effect based on magnesium microrods for combined tumor therapy, Chem. Eng. J. 446 (2022) 137038, https://doi.org/10.1016/j.cej.2022.137038.

[15] N. Yang, F. Gong, L. Cheng, H. Lei, W. Li, Z. Sun, et al., Biodegradable magnesium alloy with eddy thermal effect for effective and accurate magnetic hyperthermia ablation of tumors, Natl. Sci. Rev. 8 (1) (2021) nwaa122, https://doi.org/10.1093/nsr/nwaa122.

[16] N. Yang, F. Gong, B. Liu, Y. Hao, Y. Chao, H. Lei, et al., Magnesium galvanic cells produce hydrogen and modulate the tumor microenvironment to inhibit cancer growth, Nat. Commun. 13 (1) (2022) 2336, https://doi.org/10.1038/s41467-022-29938-6.

[17] F. Gong, J.C. Xu, B. Liu, N.L. Yang, L. Cheng, P. Huang, et al., Nanoscale CaH2 materials for synergistic hydrogen-immune cancer therapy, Chem 8 (1) (2022) 268, https://doi.org/10.1016/j.chempr.2021.11.020.

[18] H. Ge, J. Du, S. Long, X. Xia, J. Zheng, N. Xu, et al., Near-infrared light triggered H-2 generation for enhanced photothermal/photodynamic therapy against hypoxic tumor, Adv. Healthcare Mater. 11 (3) (2022) 2101449, https://doi.org/10.1002/adhm.202101449.

[19] Z. Du, X. Zhang, Z. Guo, J. Xie, X. Dong, S. Zhu, et al., X-Ray-Controlled generation of peroxynitrite based on nanosized LiLuF4:Ce3+ scintillators and their applications for radiosensitization, Adv. Mater. 30 (43) (2018) 1804046, https://doi.org/10.1002/adma.201804046.

[20] M. Aioub, S.R. Panikkanvalappi, M.A. El-Sayed, Platinum-coated gold nanorods: efficient reactive oxygen scavengers that prevent oxidative damage toward healthy, untreated cells during plasmonic photothermal therapy, ACS Nano 11 (1) (2017) 579–586, https://doi.org/10.1021/acsnano.6b06651.

[21] S. Wang, J. Huang, H. Zhu, J. Zhu, Z. Wang, Y. Xing, et al., Nanomodulators capable of timely scavenging ROS for inflammation and prognosis control following photothermal tumor therapy, Adv. Funct. Mater. 33 (21) (2023) 2213151, https://doi.org/10.1002/adfm.202213151.

[22] S. Yao, M. Zheng, Z. Wang, Y. Zhao, S. Wang, Z. Liu, et al., Self-powered, implantable, and wirelessly controlled NO generation system for intracranial neuroglioma therapy, Adv. Mater. 34 (50) (2022) 2205881, https://doi.org/10.1002/adma.202205881.

[23] B. Li, P. Ji, S.-Y. Peng, P. Pan, D.-W. Zheng, C.-X. Li, et al., Nitric oxide release device for remote-controlled cancer therapy by wireless charging, Adv. Mater. 32 (16) (2020) 2000376, https://doi.org/10.1002/adma.202000376.

[24] Z. Fang, J. Zhang, Z. Shi, L. Wang, Y. Liu, J. Wang, et al., A gas/phototheranostic nanocomposite integrates NIR-II-peak absorbing aza-BODIPY with thermal-sensitive nitric oxide donor for atraumatic osteosarcoma therapy, Adv. Mater. (2023) 2301901, https://doi.org/10.1002/adma.202301901.

[25] X. Fang, S. Cai, M. Wang, Z. Chen, C. Lu, H. Yang, Photogenerated holes mediated nitric oxide production for hypoxic tumor treatment, Angew. Chem., Int. Ed. 60 (13) (2021) 7046–7050, https://doi.org/10.1002/anie.202015082.

[26] P. Zhao, Z. Jin, Q. Chen, T. Yang, D. Chen, J. Meng, et al., Local generation of hydrogen for enhanced photothermal therapy, Nat. Commun. 9 (2018) 4241, https://doi.org/10.1038/s41467-018-06630-2.

[27] C. Li, W. Zhang, Y. Nie, X. Du, C. Huang, L. Li, J. Long, X. Wang, W. Tong, L. Qin, Y. Lai, Time-sequential and multi-functional 3D printed MgO2/PLGA scaffold developed as a novel biodegradable and bioactive bone substitute for challenging postsurgical osteosarcoma treatment, Adv. Mater. 13 (2023) 2308875.

[28] D. Wu, Y. Bai, W. Wang, H. Xia, F. Tan, S. Zhang, et al., Highly pure MgO2 nanoparticles as robust solid oxidant for enhanced Fenton-like degradation of organic contaminants, J. Hazard Mater. 374 (2019) 319–328, https://doi.org/10.1016/j.jhazmat.2019.04.058.

[29] W. Zeng, Z. Yin, M. Gao, X. Wang, J. Feng, Y. Ren, et al., In-situ growth of magnesium peroxide on the edge of magnesium oxide nanosheets: ultrahigh photocatalytic efficiency based on synergistic catalysis. Journal of Colloid and Interface *Science* 561 (2020) 257–264, https://doi.org/10.1016/j.jcis.2019.11.122.

[30] T. Seo, R. Kurokawa, B. Sato, A convenient method for determining the concentration of hydrogen in water: use of methylene blue with colloidal platinum, Medical gas Res. 2 (2012) 1–6, https://doi.org/10.1186/2045-9912-2-1.

[31] W. Ying, Y. Zhang, W. Gao, X. Cai, G. Wang, X. Wu, et al., Hollow magnetic nanocatalysts drive starvation-chemodynamic-hyperthermia synergistic therapy for tumor, ACS Nano 14 (8) (2020) 9662–9674, https://doi.org/10.1021/acsnano.0c00910.

[32] T. Luo, D. Wang, L. Liu, Y. Zhang, C. Han, Y. Xie, et al., Switching reactive oxygen species into reactive nitrogen species by photocleaved O-2-Released nanoplatforms favors hypoxic tumor repression, Adv. Sci. 8 (19) (2021) 2101065, https://doi.org/10.1002/advs.202101065.

[33] D. Hu, Y. Deng, F. Jia, Q. Jin, J. Ji, Surface charge switchable supramolecular nanocarriers for nitric oxide synergistic photodynamic eradication of biofilms, ACS Nano 14 (1) (2020) 347–359, https://doi.org/10.1021/acsnano.9b05493.